Strong quantum entanglement based on two-mode photon-subtracted squeezed vacuum states

Hongbin Song [*]

General Education Division and Shenzhen Key Laboratory of Semiconductor Lasers,
The Chinese University of Hong Kong, Shenzhen, Guang Dong 518116, China

Guofeng Zhang [†]

Department of Applied Mathematics, The Hong Kong Polytechnic University, Kowloon 999077, Hong Kong, China
and The Hong Kong Polytechnic University Shenzhen Research Institute, Shenzhen, Guang Dong 518057, China

Hidehiro Yonezawa [‡]

Centre for Quantum Computation and Communication Technology and School of Engineering and Information Technology,
The University of New South Wales, Canberra, ACT 2600, Australia

We present a strong quantum entanglement generation protocol based on two-mode photon-subtracted squeezed vacuum (TMPSSV) states. The generated entanglement shows higher entropy than those based on quantum catalysis, quantum scissors, photon-subtracted two-mode squeezed vacuum (PSTMSV) states, nonlocal PSTMSV states, and two-mode squeezed vacuum (TMSV) states in the ideal case. The impacts of experimental imperfections such as losses in the squeezed vacuum states and detection efficiency of single-photon detectors on the generated entanglement based on TMPSSV states are analyzed. When practical experimental imperfections are considered, higher logarithmic negativity than those of ideal PSTMSV states and ideal TMSV states are obtained for low initial squeezing level. Enhancement factor over 2 is obtained when the entanglement generated from imperfect non-Gaussian states passes through two lossy quantum channels in low initial squeezing level. Strong correlation is kept in lossy channels, which shows good robustness of the entanglement generation protocol based on TMPSSV states.

I. INTRODUCTION

Quantum entanglement is the nonlocal quantum correlation between two or more particles at a distance, which is originated from the Einstein, Podolsky, and Rosen (EPR) paradox [1]. Such nonlocal correlation has been created in both discrete and continuous variables (CV), which have been utilized for the test of Bell inequality violation [2–4], quantum teleportation [5–7], quantum dense coding [8,9], quantum computation [10], as well as quantum sensing [11]. Two-mode squeezed vacuum (TMSV) states are typical CV entangled states, which have been experimentally generated by combining two single-mode squeezed vacuum states with orthogonal squeezed quadratures via a balanced beam splitter as shown in Fig. 1(a) both in free space and on chips, and have been applied in quantum teleportation [7,12]. The performance of CV quantum information systems is determined by the quantum correlation between entangled particles. However, entanglement is easily degraded due to the decoherence caused by the losses in the communication channels or the storage system. Therefore, the generation of entanglement with strong quantum correlation and

robustness to losses is demanding. Various methods have been proposed to improve the quantum correlation of entangled pairs, including noiseless linear amplification [13,14], symmetric photon subtraction from two-mode squeezed vacuum (PSTMSV) states [15–17] as shown in Fig. 1(a), non-Gaussian operation on entangled modes generated from a squeezed vacuum state and a vacuum state [18], quantum catalysis as a special case of Fig. 1(a) [19], quantum scissors as shown in Fig. 1(b) [20], nonlocal single-photon subtraction from a TMSV (nonlocal PSTMSV) as illustrated in Fig. 1(c) [21], and so on. Entropy and logarithmic negativity are typical figures of merit to evaluate pure and mixed entangled states, respectively [17,20,22,23]. Entanglement enhancement with a factor less than 2 was reported based on non-Gaussian operation such as photon subtraction on entangled two-mode squeezed vacuum states (i.e., PSTMSV) reported in Ref. [17]. Quantum scissors and quantum catalysis generated entanglement with higher entropy than those based on both PSTMSV and TMSV [20]. In addition, free-propagating distilled EPR states based on noiseless linear amplification are generated with an ancilla photon [14], which demonstrated that the logarithmic negativity in a lossy channel is about five times that of TMSV. However, ancilla photons are required in quantum catalysis, quantum scissors, and noiseless linear amplification, which makes the system quite complicated.

Different from PSTMSV and nonlocal PSTMSV as shown in Figs. 1(a) and 1(c), in this work we present a protocol

---
[*]songhongbin@cuhk.edu.cn
[†]guofeng.zhang@polyu.edu.hk
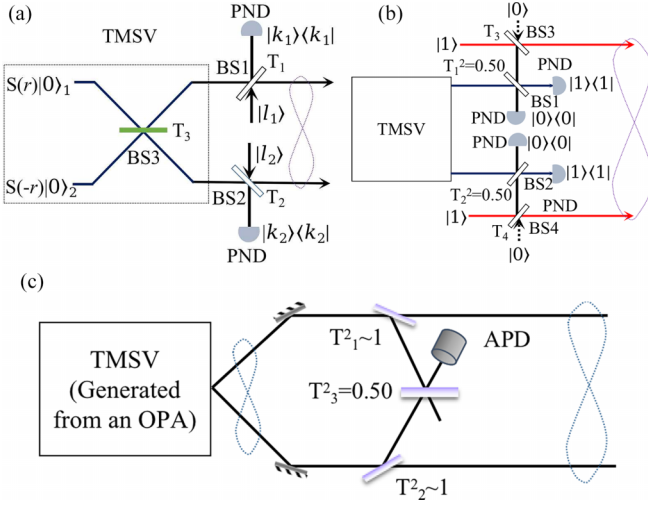[‡]h.yonezawa@unsw.edu.au

FIG. 1. Schematic diagram of entanglement generation based on (a) TMSV, PSTMSV ($l_1 = l_2 = 0$ and $k_1 = k_2 = 1$), and quantum catalysis ($l_1 = k_1$ and $l_2 = k_2$); (b) quantum scissors; and (c) nonlocal PSTMSV. BS: beam splitter; PND: photon-number detector; APD: avalanche photodiode.

to generate entanglement with two-mode photon-subtracted squeezed vacuum (TMPSSV) states as shown in Fig. 2, in which photons are subtracted from single-mode squeezed vacuum states before the entanglement is generated. The performance of the scheme is compared with entanglement improvement based on quantum scissors, PSTMSV, nonlocal PSTMSV, and TMSV in terms of entropy. In the meanwhile, mixed entanglement produced via TMPSSV with experimental imperfections is evaluated with logarithmic negativity and compared with that based on PSTMSV and TMSV.

The paper is organized as follows. In Sec. II, a general model for entanglement generation based on TMPSSV is developed. The impacts of losses in squeezed vacuum states, detection inefficiency, and loss in communication channels are
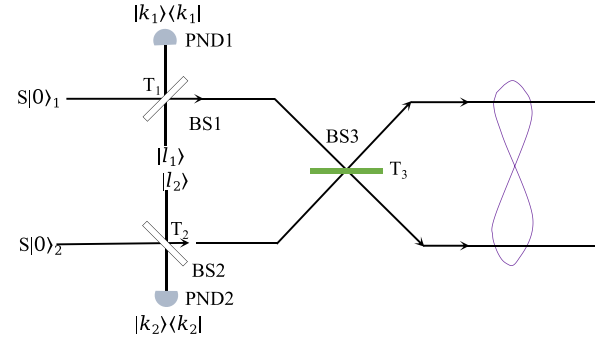

FIG. 2. Schematic diagram of entanglement generation based on TMPSSV. BS: beam splitter; PND: photon-number detector.

investigated and the performance of the protocol is compared with other schemes in Sec. III. A conclusion is provided in Sec. IV.

II. PROTOCOL FOR ENTANGLEMENT GENERATION BASED ON TMPSSV

A. General model of entanglement generation based on TMPSSV

Non-Gaussian states including Schrödinger cat states are important resources in quantum information processing, which have been successfully generated via photon subtraction from squeezed vacuum states [7,24–26]. We have developed a general model of l-photon-added and k-photon-subtracted squeezed vacuum states in Ref. [27]. As shown in Fig. 2, two non-Gaussian states are generated with l_i-photon-added and k_i-photon-subtracted squeezed vacuum states, $S|0\rangle_i$, with $i = 1, 2$. After combining the generated two non-Gaussian states with BS3, an entangled TMPSSV state is derived with tensor operation [28–31], which can be written as [27]

$$|\Psi_E\rangle = \sum_{n_1=0}^{\infty} \sum_{n_2=0}^{\infty} \gamma_{n_1, \ell_1 k_1} \gamma_{n_2, \ell_2 k_2} \sum_{j=0}^{2n_1+\ell_1-k_1} \sum_{l=0}^{2n_2+\ell_2-k_2} \gamma_{n_1,n_2,j,l} |j+l\rangle_1 |2n_1 + \ell_1 - k_1 + 2n_2 + \ell_2 - k_2 - j - l\rangle_2, \qquad (1)$$

where

$$\gamma_{n_i, l_i k_i} = \frac{\alpha_{2n_i}}{\sqrt{l_i!(2n_i)!}} \sum_{j=\max(k_i-l_i,0)}^{\min(k_i,2n_i)} \binom{l_i}{l_i - k_i + j} \binom{2n_i}{2n_i - j} \sqrt{k_i!(2n_i + l_i - k_i)!} (-1)^j T_i^{2n_i+k_i-2j} R_i^{l_i-k_i+2j}, \qquad (2)$$

$$\gamma_{n_1,n_2,j,l} \triangleq \frac{(-1)^l T_3^{2n_2+\ell_2-k_2+j-l} R_3^{2n_1+\ell_1-k_1-j+l}}{\sqrt{(2n_1+\ell_1-k_1)!(2n_2+\ell_2-k_2)!}} \binom{2n_1+\ell_1-k_1}{j} \binom{2n_2+\ell_2-k_2}{l}$$
$$\times \sqrt{(j+l)!(2n_1+\ell_1-k_1+2n_2+\ell_2-k_2-j-l)!}, \qquad (3)$$

$$\alpha_{2n_i} = \frac{1}{\sqrt{\cosh \xi_i}} \frac{\sqrt{(2n_i)!} e^{in\theta_i} \tanh^{n_i} \xi_i}{2^{n_i} n_i!}, \qquad (4)$$

where $i = 1, 2$, and ξ_i and θ_i are the squeezing parameter and squeezed angle of the input squeezed vacuum state $S|0\rangle_i$. In-phase and out-of-phase squeezed vacuum states can be obtained with $\theta_1 - \theta_2 = 0$ and $\theta_1 - \theta_2 = \frac{\pi}{2}$, respectively, which lead to in-phase and out-of-phase non-Gaussian states. T_j and R_j with $j = 1, 2, 3$ are the amplitude transmission and reflectivity of $BS\,j$ with $T_j^2 + R_j^2 = 1$.

B. Figures of merit of entanglement

Both the von Neumann entropy and the logarithmic negativity are monotone measures of entanglement [22,23]. Entropy is usually used to quantify the entanglement of pure states, while logarithmic negativity is an effective figure of merit for both pure and mixed entanglement. In an ideal case, pure entanglement could be generated. However, experimental imperfections in entanglement generation have to be considered in practice, which results in mixed entangled states. Entropy and/or logarithmic negativity are used to quantify the generated entangled states in the reported works [15–20]. To facilitate the comparison of entanglement generated from different schemes, we use both entropy and logarithmic negativity in this work.

1. Entropy for pure entangled states

For a pure two-mode state in Schmidt form, $|\Psi_{AB}\rangle = \sum_n c_n |a_n\rangle_A |b_n\rangle_B$, the von Neumann entropy is defined as [18,32]

$$
\begin{aligned}
E &= -\text{Tr}(\rho_A \log_2 \rho_A) \\
&= -\text{Tr}(\rho_B \log_2 \rho_B) \\
&= -\sum_n c_n^2 \log_2 c_n^2,
\end{aligned}
\tag{5}
$$

where $\rho_A = \text{Tr}_B(\rho_{AB}) = \sum_n c_n^2 |a_n\rangle\langle a_n|$, $\rho_B = \text{Tr}_A(\rho_{AB}) = \sum_n c_n^2 |b_n\rangle\langle b_n|$, and $\rho_{AB} = |\Psi_{AB}\rangle\langle\Psi_{AB}|$. In terms of TMSV, the von Neumann entropy can be derived as [20] $E_{\text{TMSV}} = \cosh^2\xi \log_2 \cosh^2\xi - \sinh^2\xi \log_2 \sinh^2\xi$, where ξ is the initial squeezing parameter. The entropy of the quantum entangled state shown in Eq. (1) can be obtained based on Eq. (5) with $\rho_{AB} = |\Psi_E\rangle\langle\Psi_E|$. When $l_1 = l_2 = 0$ and $k_1 = k_2 = 1$ in Fig. 2, i.e., when one photon is subtracted from each of these two single-mode squeezed vacuum states, two non-Gaussian states (also called Schrödinger kitten states) are obtained. Combining these non-Gaussian states with BS3, a TMPSSV state is produced, in which the two modes are entangled. The entropy variation of the entangled states generated via TMPSSV, a quantum scissor, and TMSV are shown in Fig. 3 when the squeezing parameter $\xi = 0.10$ (i.e., -0.87 dB), $\xi = 0.40$ (i.e., -3.47 dB), and $\xi = 0.70$ (i.e., -6.08 dB). The transmissions of BS3 in TMSV, PSTMSV, and TMPSSV are all denoted as T_3 as shown in Figs. 1(a) and 2, while $T_3 = T_4$ in the case of quantum scissors in Fig. 1(b). According to Eq. (1), when the initial squeezing is weak, two kitten states are equivalent to two single photons. Thus, we can obtain a qutrit state described as

$$
\begin{aligned}
|\Psi_E\rangle = {}&\sqrt{2}T_3 R_3 (|02\rangle - e^{-2i\phi}|20\rangle) \\
&+ (T_3^2 - R_3^2) e^{-i\phi}|11\rangle + o(\xi),
\end{aligned}
\tag{6}
$$

where ϕ is the phase difference between two non-Gaussian states. The maximum qutrit entangled state, $|02\rangle + |20\rangle + |11\rangle$, with an entropy over 1 will be obtained when all coefficients have the same magnitude, which requires T_3 to satisfy $\sqrt{2}T_3\sqrt{1-T_3^2} = 2T_3^2 - 1$, i.e., $T_3^2 = 0.21$ or $T_3^2 = 0.79$. As shown in Fig. 3(a), the transmission of BS3 for both in-phase and out-of-phase Schrödinger kitten states is optimized at $T_3^2 = 0.21$ and $T_3^2 = 0.79$ with the maximum entropy, which

well matches the prediction in theory; while in the case of quantum scissors, only the maximum entangled qubit state $|01\rangle + |10\rangle$ is possibly generated, thus its entropy cannot go beyond 1 even with optimized parameters.

With the increase of the initial squeezing, similar to TMSV, T_3^2 is optimized at $T_3^2 = 0.5$ for the scheme with two out-of-phase Schrödinger kitten states, while the optimization of $T_3^2 = 0.21$ and 0.79 is obtained in the case of in-phase kitten states. Thus, comparing with TMSV, TMPSSV shows better flexibility to generate strong entanglement with an extra degree of freedom. In addition, when the initial squeezing is increased, the scheme with two out-of-phase Schrödinger kitten states outperforms that of two in-phase Schrödinger kitten states, quantum scissors, and TMSV. As out-of-phase kitten states haver better performance than the in-phase case when the initial squeezing is increased, we will focus on the entanglement generation based on out-of-phase non-Gaussian states in the following discussion.

Figure 4 shows the variation of entropy with the initial squeezing parameter ξ for different schemes, TMPSSV, quantum scissors, PSTMSV, nonlocal PSTMSV, and TMSV. The pink line describes the case of TMPSSV with two out-of-phase kitten states and $T_3^2 = 0.50$. The blue crosses and red squares represent the quantum scissors shown in Fig. 2 with the optimized transmission of BS3 and BS4 of $T_3^2 = T_4^2 = T^2$ and $T_3^2 = T_4^2 = T^2 = 0.80$ for each initial squeezing parameter ξ, respectively. The purple squares, orange plus, and green dot-dashed line denote the scheme of PSTMSV, nonlocal PSTMSV, and TMSV, respectively. The energy transmission of the beam splitters, BS1 and BS2, for single-photon subtraction in PSTMSV and nonlocal PSTMSV shown in Figs. 1(a) and 1(c) are taken as $T_1^2 = T_2^2 = 0.95$. It can be seen that entanglement generated from TMPSSV with two out-of-phase kitten states has higher entropy than those generated from quantum scissors, quantum catalysis (shown in Ref. [20]), and TMSV in the full range of the initial squeezing $\xi \in (0, 1]$ since a higher dimensional quantum state with larger maximum entanglement could be generated in TMPSSV as indicated by Eq. (6). When $\xi \leqslant 0.32$ (i.e., -2.78 dB), nonlocal PSTMSV has larger entropy than PSTMSV. Whereas when $\xi \leqslant 0.60$ (i.e., -5.30 dB), TMPSSV with two out-of-phase kitten states performs better than PSTMSV. Therefore, the entanglement generated from TMPSSV shown in Fig. 2 outperforms nonlocal PSTMSV, quantum catalysis, quantum scissors, PSTMSV, and TMSV. In particular, when the initial squeezing is extremely weak, Schrödinger kitten states generated from single-photon subtracted squeezed vacuum states approach single-photon states. When such two single photons are combined by BS3 with $T^2 = 0.50$, the generated entangled state approaches a Bell state with maximum entanglement $\frac{|02\rangle + |20\rangle}{\sqrt{2}}$ due to the Hong-Ou-Mandel effect. A Bell state of $\frac{|01\rangle - |10\rangle}{\sqrt{2}}$ can be obtained in the case of nonlocal PSTMSV, which causes the same entropy with TMPSSV; while only vacuum modes are available in the case of TMSV and PSTMSV. With the increase of the initial squeezing level, a qutrit state indicated by Eq. (6) is generated, which leads to higher entropy than that of nonlocal PSTMSV and TMPSSV. Therefore, the entanglement generation based TMPSSV shown in Fig. 2 implies stronger quantum correlation than other schemes.
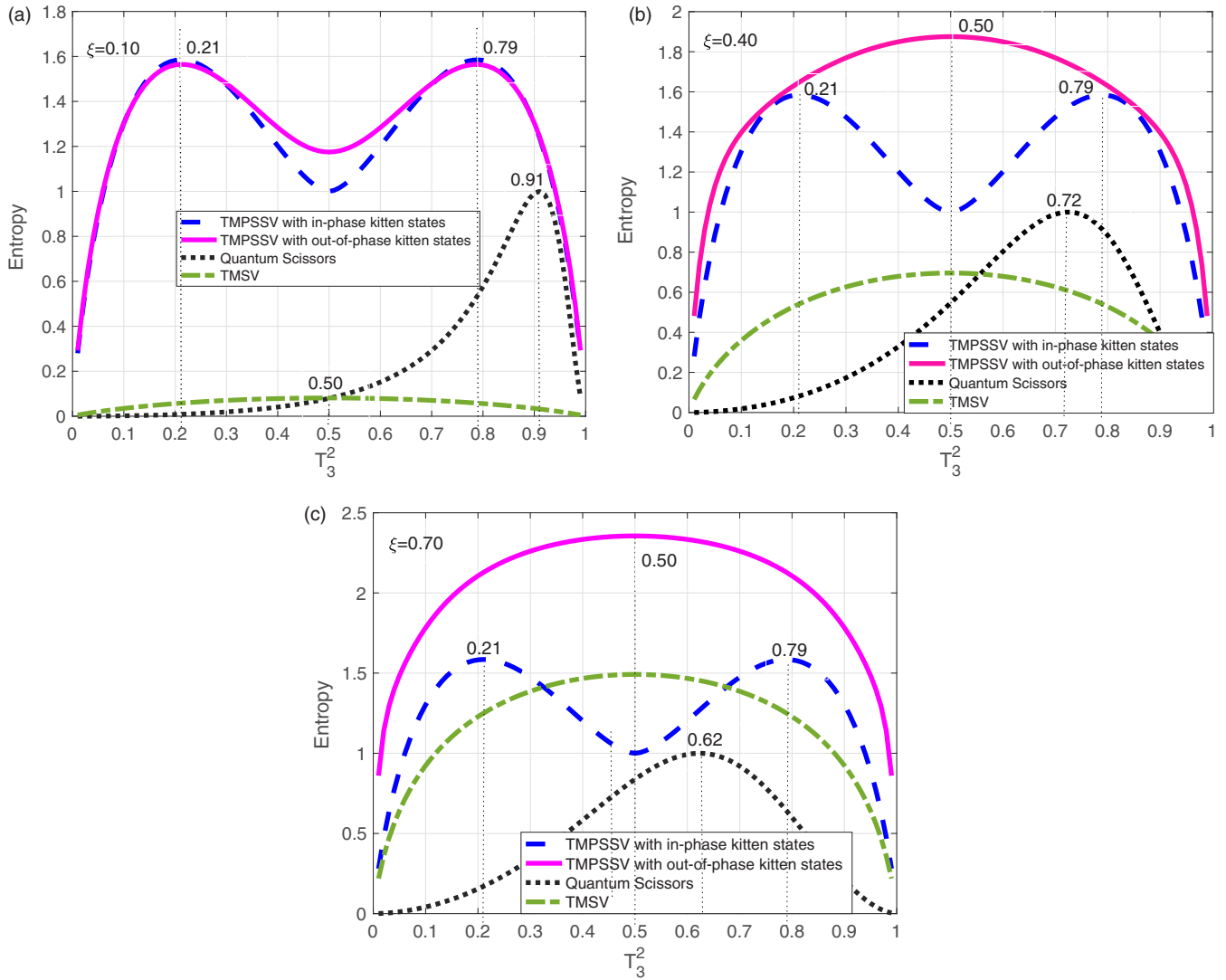
FIG. 3. Variation of entropy with T_3^2 in TMPSSV with in-phase and out-of-phase kitten states and quantum scissor with different squeezing parameters (a) $\xi = 0.10$, (b) $\xi = 0.40$, and (c) $\xi = 0.70$.
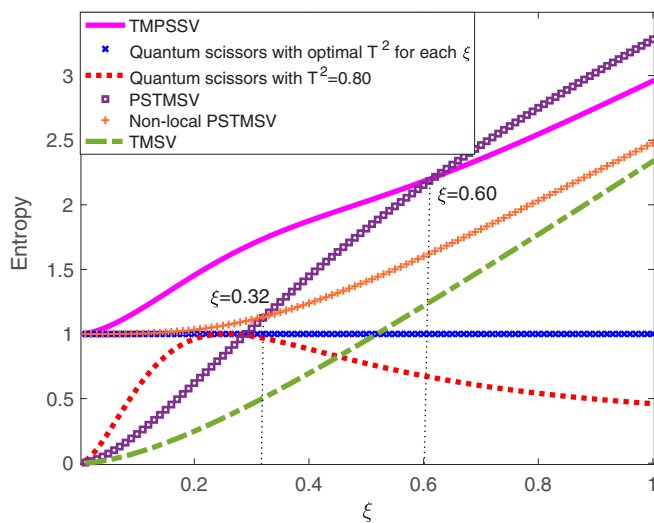

FIG. 4. Comparison of entropy in different schemes.

It is worth noting that conditional measurement is involved in nonlocal PSTMSV, PSTMSV, and TMPSSV for single-photon subtraction. Success probabilities (in logarithmic scale) of entanglement based on nonlocal PSTMSV, PSTMSV, and TMPSSV are shown in Fig. 5. Nonlocal PSTMSV shows the highest success probability since only one photon is subtracted from two correlated modes; while in the cases of two single-photon subtraction on both modes, PSTMSV shows a higher success probability than that of TMPSSV because two single photons are subtracted from two correlated modes of TMSV in PSTMSV. It is indicated that the single-photon subtraction order causes a difference in the success probability of entanglement generation. Although the success probability of TMPSSV is relatively lower, a stronger correlation between two parties can be achieved, which is very critical to enhance the performance of a quantum information system. In addition, compared with the schemes of nonlocal PSTMSV and PSTMSV with a fixed $T_3^2 = 0.50$, an extra degree of freedom, i.e., a variable T_3, is available to achieve
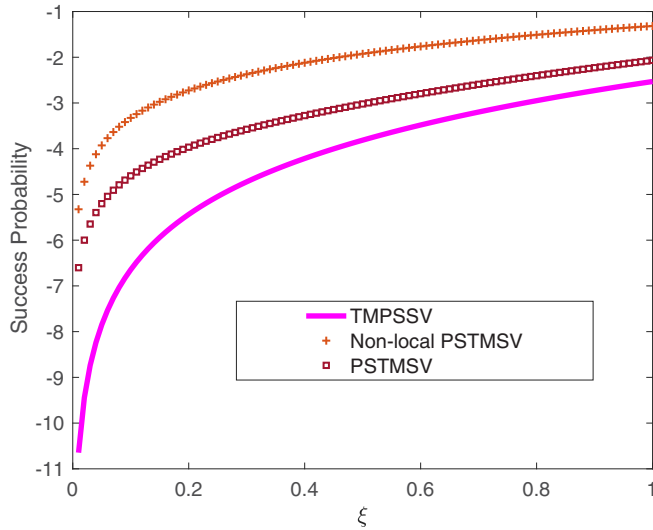
FIG. 5. Comparison of success probability in TMPSSV, nonlocal PSTMSV, and PSTMSV.

higher entanglement in TMPSSV for lower initial squeezing as shown in Fig. 3(a).

2. Logarithmic negativity

Logarithmic negativity of a bipartite state ρ_{AB} is defined as [22]

$$E_N = \log_2 \|\rho_{AB}^{\text{PT}}\|, \tag{7}$$

where ρ_{AB}^{PT} is the partial transpose of the bipartite, and $\|\rho_{AB}^{\text{PT}}\| = \text{Tr}[\sqrt{\rho_{AB}^{\text{PT}} * \rho_{AB}^{\text{PT}\dagger}}]$ is the trace norm of the partial transpose of ρ_{AB}. For a pure entanglement generated from TMSV, the logarithmic negativity can be derived as [17]

$$E_N^{\text{TMSV}} = \log_2\left[\frac{1+\lambda}{1-\lambda}\right], \tag{8}$$

where $\lambda = \tanh\xi$ with ξ being the squeezing parameter. In terms of PSTMSV, i.e., symmetrically subtracted one photon from each mode of TMSV, the logarithmic negativity is derived as [33]

$$E_N^{\text{PSTMSV}} = 2\log_2\left[\frac{1+\lambda T}{1-\lambda T}\sqrt{\frac{1-\lambda^2 T^2}{1+\lambda^2 T^2}}\right]. \tag{9}$$

3. Logarithmic negativity of entanglement generated from TMPSSV

To generalize the model of entanglement based on TMPSSV shown in Fig. 2, two input non-Gaussian states can be written as

$$\rho_1 = \sum_{m,n=0}^{\infty} \alpha_{mn}|m\rangle\langle n|, \qquad \rho_2 = \sum_{p,q=0}^{\infty} \beta_{pq}|p\rangle\langle q|, \tag{10}$$

and the density matrix of the generated entangled state after BS3 can be described as [27]

$$\rho_{AB} = \sum_{m,p=0}^{\infty}\sum_{n,q=0}^{\infty} \frac{\alpha_{mn}\beta_{pq}}{\sqrt{m!n!p!q!}} \sum_{j_1=0}^{m}\sum_{i_1=0}^{p}\sum_{j_2=0}^{n}\sum_{i_2=0}^{q} \binom{m}{j_1}\binom{p}{i_1}\binom{n}{j_2}\binom{q}{i_2}(-1)^{i_1+i_2}T_3^{p+q+j_1+j_2-i_1-i_2}R_3^{m+n+i_1+i_2-j_1-j_2}$$
$$\times \sqrt{(j_1+i_1)!(j_2+i_2)!(m+p-j_1-i_1)!(n+q-j_2-i_2)!}\,|j_1+i_1\rangle|m+p-j_1-i_1\rangle\langle n+q-j_2-i_2|\langle j_2+i_2|. \tag{11}$$

The partial transpose of ρ_{AB} is derived as

$$\rho_{AB}^{\text{PT}} = \sum_{m,p=0}^{\infty}\sum_{n,q=0}^{\infty} \frac{\alpha_{mn}\beta_{pq}}{\sqrt{m!n!p!q!}} \sum_{j_1=0}^{m}\sum_{i_1=0}^{p}\sum_{j_2=0}^{n}\sum_{i_2=0}^{q} \binom{m}{j_1}\binom{p}{i_1}\binom{n}{j_2}\binom{q}{i_2}(-1)^{i_1+i_2}T_3^{p+q+j_1+j_2-i_1-i_2}R_3^{m+n+i_1+i_2-j_1-j_2}$$
$$\times \sqrt{(j_1+i_1)!(j_2+i_2)!(m+p-j_1-i_1)!(n+q-j_2-i_2)!}\,|j_2+i_2\rangle_A\langle j_1+i_1| \otimes |m+p-j_1-i_1\rangle_B\langle n+q-j_2-i_2|. \tag{12}$$

According to Refs. [22,34], the trace norm is simply the sum of the absolute value of eigenvalues of ρ_{AB}^{PT} since ρ_{AB}^{PT} is Hermitian. Therefore, the logarithmic negativity of the entanglement generated from TMPSSV can be numerically obtained.

Figure 6 compares the logarithmic negativity of the entanglement generated from single-photon-subtracted squeezed vacuum states ($l_1 = l_2 = 0$, $k_1 = k_2 = 1$), single-photon-added squeezed vacuum states ($l_1 = l_2 = 1$, $k_1 = k_2 = 0$), single-photon-added and two-photon-subtracted squeezed vacuum states (i.e., $l_1 = l_2 = 1$, $k_1 = k_2 = 2$), two-photon-added and one-photon-subtracted squeezed vacuum states (i.e., $l_1 = l_2 = 2$, $k_1 = k_2 = 1$), as well as single-photon-added and single-photon-subtracted squeezed vacuum states (i.e., $l_1 = l_2 = 1$ and $k_1 = k_2 = 1$) with those generated from PSTMSV and TMSV. It indicated that the first four schemes perform better than both PSTMSV and TMSV in lower initial squeezing. Single-photon addition (i.e., $l_1 = l_2 = 1$ and $k_1 = k_2 = 0$ indicated by a pink line) and single-photon subtraction (i.e., $l_1 = l_2 = 0$ and $k_1 = k_2 = 1$ described by a dashed blue line) from squeezed vacuum states lead to equivalent entanglement, since both generate squeezed single-photon states [35]; while the logarithmic negativity of entanglement generated from two-photon-added and one-photon-subtracted squeezed vacuum states (i.e., $l_1 = l_2 = 2$, $k_1 = k_2 = 1$ denoted by diamond symbols) is higher than that from one-photon-added and two-photon-subtracted squeezed vacuum states (i.e., $l_1 = l_2 = 1$, $k_1 = k_2 = 2$ indicated by square symbols). In addition, single-photon-added
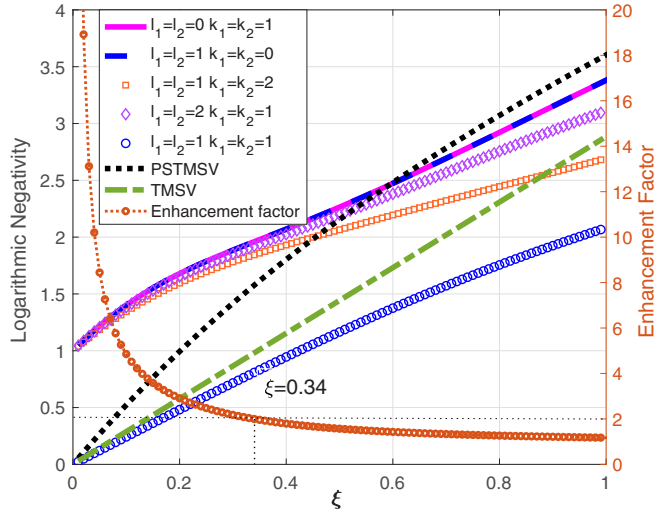
FIG. 6. Logarithmic negativity of entanglement generated from different schemes.

FIG. 7. Comparison of logarithmic negativity in different schemes.

and single-photon-subtracted (i.e., $l_1 = l_2 = 1$ and $k_1 = k_2 = 1$ described by circle symbols) squeezed vacuum states are equivalent to the quantum catalysis operation on two single-mode squeezed vacuum states, which has lower logarithmic negativity than that of PSTMSV and TMSV. It implied that quantum catalysis on each mode of TMSV is helpful to enhance entanglement, while such operation on two single-mode squeezed vacuum states before an entanglement is generated does not work. It is noticed that the entanglement generated with photon addition (i.e., $l_i \neq 0$, $i = 1$ and 2) does not show better performance with more complicated operation. Therefore, it will help us to select a good-quality entanglement generation scheme with simpler non-Gaussian operation, i.e., single-photon-subtracted operation on squeezed vacuum states, i.e., $l_1 = l_2 = 0$, $k_1 = k_2 = 1$. This is quite helpful to construct the experimental setup in practice.

Furthermore, the enhancement factor, defined as the ratio between the logarithmic negativity of entanglement generated from two kitten states (i.e., $l_1 = l_2 = 0$ and $k_1 = k_2 = 1$) and TMSV, is shown in Fig. 6 via the orange dotted line with circle symbols. It indicates that an enhancement factor over 2 can be obtained when $\xi < 0.34$ (i.e., -2.95 dB), which breaks the factor limit of 2 in PSTMSV mentioned in Ref. [14]. In addition, the lower the initial squeezing, the higher enhancement factor in entanglement generated from TMPSSV.

According to the examination of the photon addition and subtraction operation on two single-mode squeezed vacuum states in TMPSSV, we concluded that photon subtraction (i.e., $l_1 = l_2 = 0$ and $k_1 = k_2 \neq 0$) has better performance in producing entanglement in TMPSSV. Thus, we will stick to photon-subtracted squeezed vacuum states in the following. Besides single-photon-subtracted squeezed vacuum states, the non-Gaussian states shown in Fig. 2 can also be generated by subtracting multiple photons such as $k_1 = k_2 > 1$. The logarithmic negativity of entangled states generated from symmetric non-Gaussian states, i.e., $l_1 = l_2 = 0$ and $k_1 = k_2 = 1, 2, 3, 4$, are shown in Fig. 7 and compared with those generated from PSTMSV and TMSV. Figure 7 implies
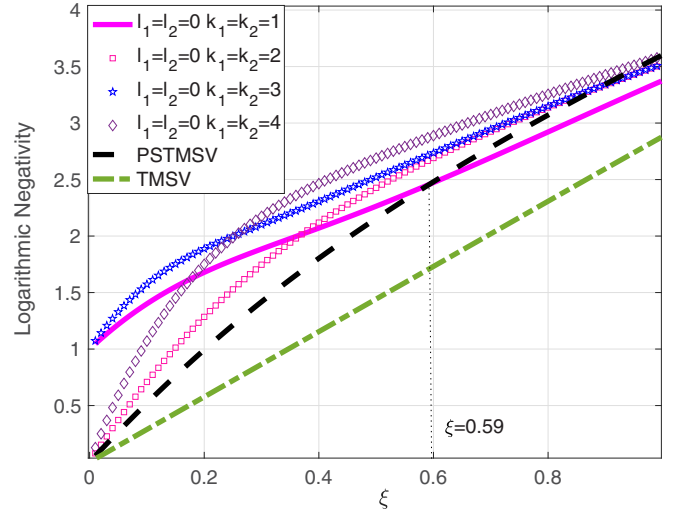
that entanglement generated from non-Gaussian states has higher logarithmic negativity than TMSV in the whole range of squeezing parameters. When $\xi \leqslant 0.59$ (i.e., -5.12 dB), single-photon subtraction on two single-mode squeezed vacuum states (TMPSSV with $l_1 = l_2 = 0$ and $k_1 = k_2 = 1$) shows better performance than single-photon subtraction from TMSV, i.e., PSTMSV. In addition, with the increase of subtracted photon number, the enhancement of entanglement becomes more significant. Odd-photon subtractions, e.g., $k_1 = k_2 = 1$ and 3, demonstrate better performance in the lower initial squeezing region, while even-photon subtractions, e.g., $k_1 = k_2 = 2$ and 4, outperform in the higher initial squeezing region. However, the more photons are subtracted, the more complicated the experimental setup. Therefore, as a typical example, we will focus on $l_1 = l_2 = 0$ and $k_1 = k_2 = 1$ in the following discussions.

III. IMPACTS OF EXPERIMENTAL IMPERFECTIONS

Similar to Schrödinger kitten states generation [36], when a non-Gaussian state is generated based on k-photon subtraction from a squeezed vacuum state, $S|0\rangle$, the experimental imperfections including loss in squeezed vacuum states, photon-number-resolving ability, detection inefficiency, and dark counts of photon-number detectors will degrade the purity of the non-Gaussian states. As a result, mixed non-Gaussian states are produced, which will affect the entanglement generated in the subsequent step shown in Fig. 2. In addition, the loss in communication channels will degrade the entanglement further. Therefore, all imperfections should be considered to investigate the feasibility of the entanglement generation based on TMPSSV. Fortunately, the rapid development of photon-number detection techniques offers a solution to the problem of photon-number-resolving ability. Furthermore, the dark counts could be decreased to be negligible, and detection efficiency as high as 98% is achievable in superconducting transition-edge sensors (TESs) [27,37]. Without loss of generality, we will consider the loss in two squeezed vacuum states, γ_i ($i = 1, 2$), single-photon detection efficiency, η_{SPDi} ($i = 1, 2$), and losses in both communication
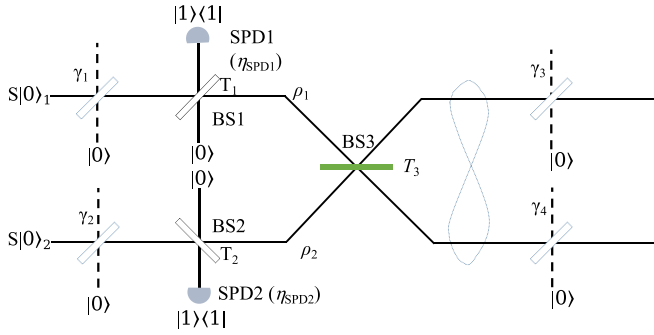
FIG. 8. Schematic diagram of entanglement generation based on TMPSSV. BS: beam splitter; SPD: single-photon detector.

channels, γ_3 and γ_4. Losses in both squeezed vacuum states and communication channels, γ_i ($i = 1, 2, 3, 4$), can be equivalent to the energy reflectivity of imaginary beam splitters as shown in Fig. 8. We will discuss the impact of γ_i ($i = 1, 2$) and

η_{SPD} first. Then the impact of the losses in the communication channels, γ_3 and γ_4, will be analyzed.

A. Impact of the loss in squeezed vacuum states and the detection efficiency of single-photon detector

In this part, we will analyze the impact of losses in the initial squeezed vacuum states, γ_i ($i = 1, 2$), and the detection efficiency of single-photon detectors for single-photon subtraction, $\eta_{\text{SPD}i}$ ($i = 1, 2$). According to the model developed in Ref. [27], the loss of squeezed vacuum states, γ_i, and the detection efficiency of a single-photon detector (SPD), $\eta_{\text{SPD}i}$ ($i = 1, 2$), result in mixed non-Gaussian states, which can be represented by ρ_1 and ρ_2. Then the entangled state output from BS3 is derived as Eq. (11) [27]. As a result, the logarithmic negativity of the entanglement generated from the scheme shown in Fig. 8 can be obtained based on the partial transpose derived in Eq. (12).

Figure 9 indicates the variation of the logarithmic negativity as a function of T_3 with the initial squeezing parameter
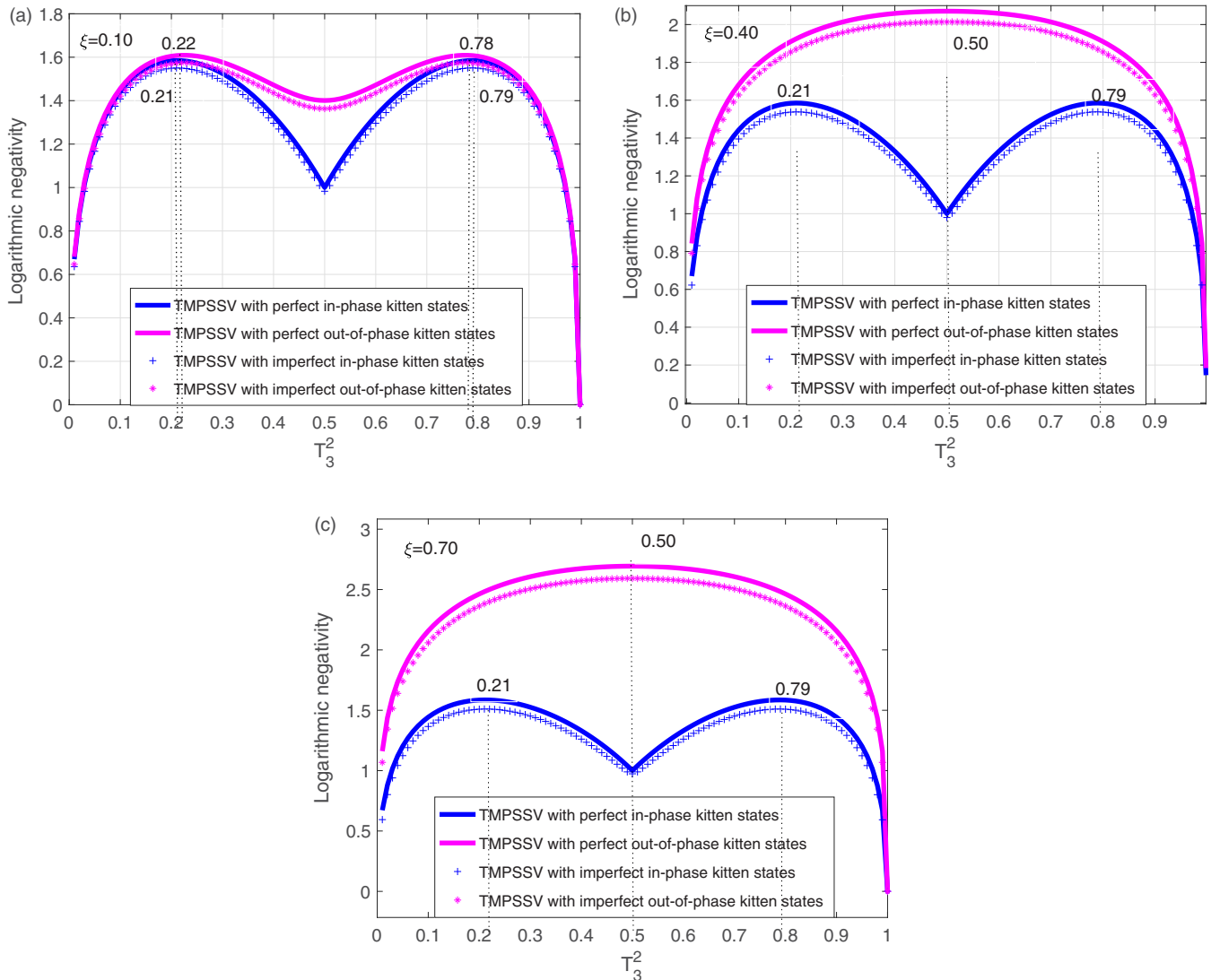

FIG. 9. Variation of logarithmic negativity with T_3 in TMPSSV generated from perfect and imperfect kitten states with squeezing parameters of (a) $\xi = 0.10$, (b) $\xi = 0.40$, and (c) $\xi = 0.70$, $T_1^2 = T_2^2 = 0.95$ and $\gamma = 0.01$, $\eta_{\text{SPD}} = 0.98$ for imperfect kitten states.
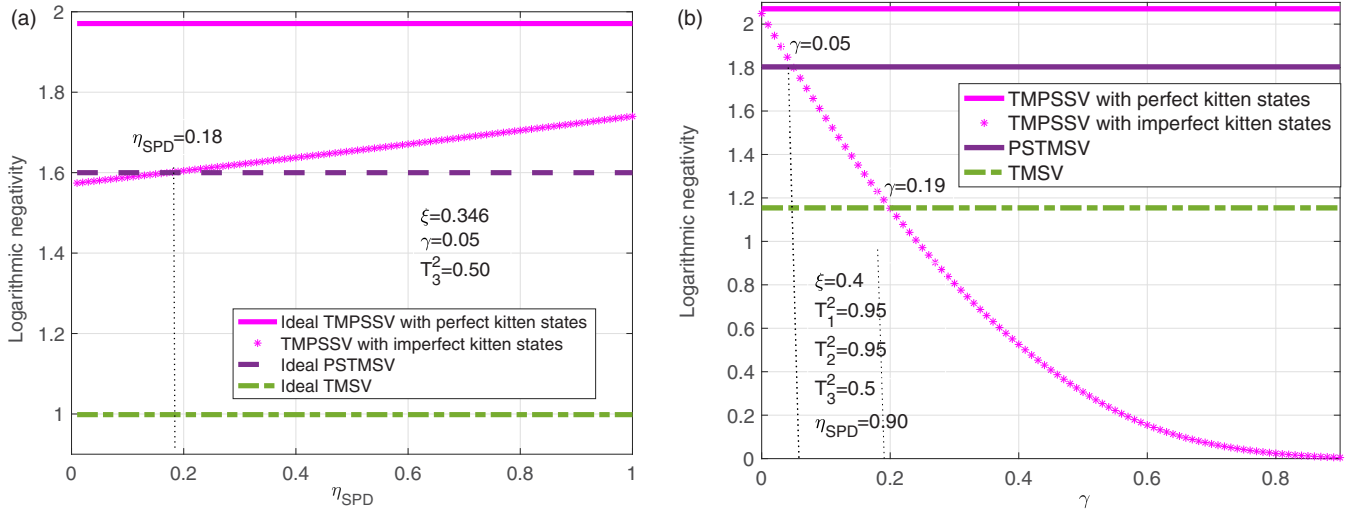
FIG. 10. Variation of logarithmic negativity with (a) the detection efficiency of SPDs when $\xi = 0.346$, $\gamma = 0.10$; (b) the loss in the initial squeezed vacuum states γ when $\xi = 0.40$ and $\eta_{\mathrm{SPD}} = 0.90$.

ξ when $\gamma_1 = \gamma_2 = 0.01$ and $\eta_{\mathrm{SPD1}} = \eta_{\mathrm{SPD2}} = \eta = 0.98$. As expected, the logarithmic negativity in both in-phase and out-of-phase kitten states is decreased. When $\xi = 0.10$, the transmission of BS3 is optimized at $T_3^2 = 0.22$ and $T_3^2 = 0.78$ as shown in Fig. 9(a), which is slightly different from the perfect case. With the increase of the initial squeezing, T_3^2 is optimized as $T_3^2 = 0.50$ for out-of-phase kitten states when $\xi = 0.40$ and $\xi = 0.70$ as indicated in Figs. 9(b) and 9(c); while the experimental imperfections do not change the optimized value of T_3^2 for two in-phase kitten states in the full range of initial squeezing levels. Therefore, $T_3^2 = 0.50$ is utilized in the entanglement generation based on non-Gaussian states in the following discussion. The impact of loss in the initial squeezed vacuum states, $\gamma_1 = \gamma_2 = \gamma$, and the detection efficiency, $\eta_{\mathrm{SPD1}} = \eta_{\mathrm{SPD2}} = \eta_{\mathrm{SPD}}$, are analyzed as shown in Fig. 10. When $\xi = 0.346$ (i.e., -3.00 dB) and $\gamma = 0.05$, the logarithmic negativity of entanglement generated from imperfect non-Gaussian states is larger than both ideal PSTMSV and TMSV as long as $\eta_{\mathrm{SPD}} \geqslant 0.18$ as shown in Fig. 10(a). Comparing with the influence of the loss in the initial squeezing shown in Fig. 10(b), the influence of single-photon detection efficiency on the logarithmic negativity is quite weak. In practice, a TES with detection efficiency over 0.90 is commercially available [37]. Thus, the impact of the detection efficiency of single-photon detectors could be compensated. When $\xi = 0.40$ (i.e., -3.47 dB), $\eta_{\mathrm{SPD}} = 0.90$, the initial squeezing loss, $\gamma \leqslant 0.05$, is required to keep the logarithmic negativity of entanglement generated from imperfect non-Gaussian states larger than those of ideal PSTMSV and TMSV as shown in Fig. 10(b). The loss of squeezed vacuum states could be controlled as low as $\gamma \leqslant 0.05$ in experiments at both 860 and 1550 nm [38,39], which facilitates the implementation of the protocol in practice.

Figure 11 shows the variation of logarithmic negativity of entanglement with the initial squeezing parameter ξ. The purple asterisk and violet circles represent entanglement generated from TMPSSV with two imperfect kitten states of $\gamma = 0.01$, $\eta_{\mathrm{SPD}} = 0.90$ as well as $\gamma = 0.03$, $\eta_{\mathrm{SPD}} = 0.45$, respectively. The pink line, orange cross, dotted blue line,

and dash-dotted green line describe the logarithmic negativity of entanglement generated from perfect TMPSSV, perfect nonlocal PSTMSV, perfect PSTMSV, and perfect TMSV. It implies that when $\gamma = 0.01$, $\eta_{\mathrm{SPD}} = 0.90$, entanglement based on TMPSSV outperforms ideal nonlocal PSTMSV and TMSV in the whole range of $\xi \in (0, 1]$ and performs better than PSTMSV as long as $\xi \leqslant 0.51$ (i.e., -4.43 dB). In a more realistic case, i.e., $\gamma = 0.03$, $\eta_{\mathrm{SPD}} = 0.45$, TMPSSV shows stronger entanglement than ideal TMSV, ideal nonlocal PSTMSV, and ideal PSTMSV when $\xi \leqslant 0.85$ (i.e., -7.38 dB), $\xi \leqslant 0.70$ (i.e., -6.08 dB), and $\xi \leqslant 0.40$ (i.e., -3.47 dB), which indicates the good robustness and feasibility of TMPSSV.

B. Losses in the communication channels

With the influence of experimental imperfections in TMPSSV, the generated entanglement state is a mixed
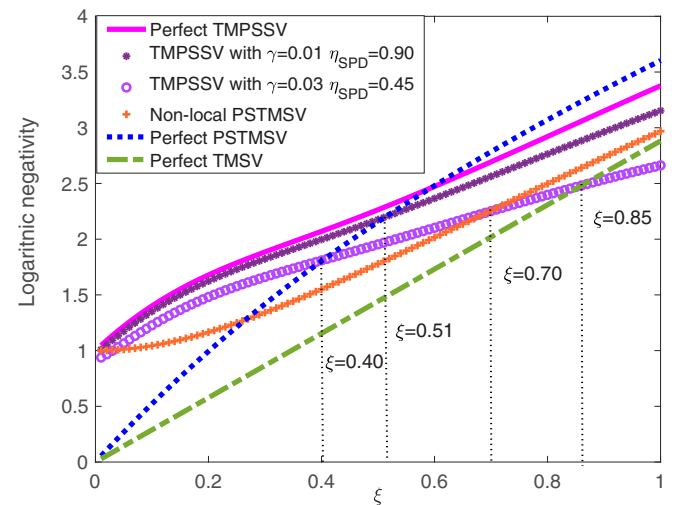

FIG. 11. Variation of logarithmic negativity with the initial squeezed parameter ξ when $\gamma = 0.01$, $\eta_{\mathrm{SPD}} = 0.90$ and $\gamma = 0.03$, $\eta_{\mathrm{SPD}} = 0.45$.

rather than a pure state. Without loss of generality, the case of an impure entanglement state, denoted by $\rho_{AB} = \sum_{m,n,j,k=0} c_{mnjk}|m,n\rangle\langle j,k|$, is considered. Loss in a channel is equivalent to the reflectivity coefficient of an imaginary beam splitter as shown in Fig. 8, in which γ_3 and γ_4 are the loss of the channel for particle A and B, respectively. After passing through lossy channels, the density matrix of the entangled state is derived as

$$\rho_{\text{outloss}\,E} = \sum_{m,n}\sum_{j,k}\sum_{j_1=0}^{\min(m,k)}\sum_{j_2=0}^{\min(n,j)} c_{mnjk}\sqrt{\binom{m}{j_1}\binom{n}{j_2}\binom{j}{j_2}\binom{k}{j_1}}(1-\gamma_3)^{(m+k-2j_1)/2}$$
$$\times \gamma_3^{j_1}(1-\gamma_4)^{(n+j-2j_2)/2}\gamma_4^{j_2}|m-j_1\rangle_A\langle k-j_1|\otimes|n-j_2\rangle_B\langle j-j_2|. \tag{13}$$

The partial transpose of $\rho_{\text{outloss}\,E}$ can be derived as

$$\rho_{\text{outloss}\,E}^{PT} = \sum_{m,n}\sum_{j,k}\sum_{j_1=0}^{\min(m,k)}\sum_{j_2=0}^{\min(n,j)} c_{mnjk}\sqrt{\binom{m}{j_1}\binom{n}{j_2}\binom{j}{j_2}\binom{k}{j_1}}(1-\gamma_3)^{(m+k-2j_1)/2}$$
$$\times \gamma_3^{j_1}(1-\gamma_4)^{(n+j-2j_2)/2}\gamma_4^{j_2}|k-j_1\rangle_A\langle m-j_1|\otimes|n-j_2\rangle_B\langle j-j_2|. \tag{14}$$

Therefore, the logarithmic negativity of the entanglement through two lossy channels can be analyzed. When the losses of the communication channels are $\gamma_3 = \gamma_4 = 0.05$, degradations in the logarithmic negativity for entanglement generated from two imperfect kitten states with $\gamma_1 = \gamma_2 = 0.03$ and $\eta_{\text{SPD1}} = \eta_{\text{SPD2}} = 0.45$ are compared with that of ideal PSTMSV and imperfect TMSV as shown in Fig. 12. It is indicated that imperfect TMPSSV propagating in lossy channels has higher logarithmic negativity than that of an ideal PSTMSV traveling in lossless communication channels when $\xi \leqslant 0.40$ (i.e., -3.47 dB). Furthermore, when $\xi \leqslant 0.90$ (i.e., -7.82 dB), TMSV shows a stronger correlation than that of TMSV when both experimental imperfections and losses in channels are considered.

In addition, the enhancement factors defined as the ratio between the generated entanglement based on non-Gaussian states and TMSV in a lossless/lossy channel are investigated as shown in the right y axis of Fig. 12. The enhancement factor of 2 can be obtained when $\xi < 0.30$ (i.e., -2.61 dB) in both loss and lossless communication channels. The lower

the initial squeezing the higher enhancement factor, which reveals a stronger correlation between entangled particles based on TMPSSV. Therefore, TMPSSV provides an approach to generate high-quality quantum resource for long-distance communication.

IV. CONCLUSION

In conclusion, a protocol to generating an entangled state based on TMPSSV is proposed and evaluated. Two non-Gaussian states produced from l-photon-added and k-photon-subtracted squeezed vacuum states are combined with a beam splitter. Two-mode non-Gaussian entanglement with stronger nonlocal quantum correlation than that from quantum scissors, quantum catalysis, nonlocal PSTMSV, PSTMSV, and TMSV is predicted when $l = 0$ and $k = 1$, i.e., the non-Gaussian states are Schrödinger kitten states in the case of a balanced BS3, i.e., $T_3^2 = 0.50$. In addition, much stronger entanglement can be achieved in TMPSSV when $T_3^2 = 0.21$ in lower initial squeezing levels, which indicates that TMPSSV is more flexible with an extra degree of freedom T_3 than PSTSMV, nonlocal PSTMSV, and TMSV since $T_3^2 = 0.50$ is required in all these schemes. A general model embedding experimental imperfections in the Schrödinger kitten states generation and lossy channels during the propagation of the entangled state is developed. Entanglement generated from TMPSSV shows stronger entanglement than an ideal nonlocal PSTMSV, PSTMSV, and TMSV when all imperfections are considered, including losses in the initial squeezed vacuum states, detection inefficiency of single-photon detectors, and losses in the quantum channels.

Therefore, the protocol provides a quantum resource with stronger nonlocal correlation for quantum information processing, in particular long-distance quantum communication and quantum metrology.
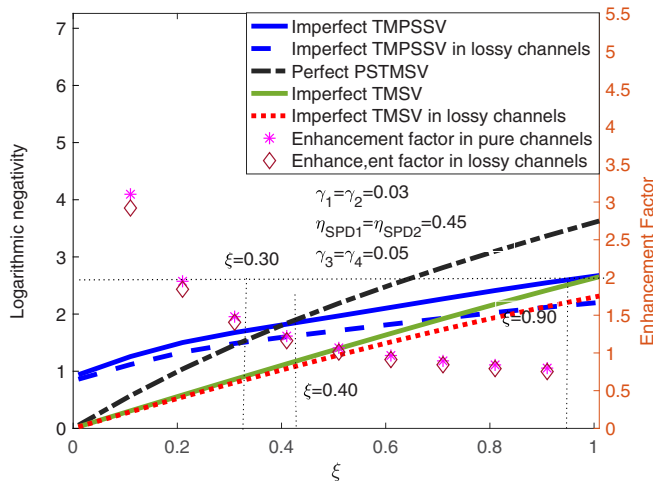

FIG. 12. Logarithmic negativity and enhancement factor of entanglement in lossy and lossless channels with $\gamma_1 = \gamma_2 = 0.03$, $\eta_{SPD1} = \eta_{SPD2} = 0.45$ and $\gamma_3 = \gamma_4 = 0.05$.

ACKNOWLEDGMENTS

[1] A. Einstein, B. Podolsky, and N. Rosen, Can quantum-mechanical description of physical reality be considered complete? Phys. Rev. **47**, 777 (1935).

[2] G. Weihs, T. Jennewein, C. Simon, H. Weinfurter, and A. Zeilinger, Violation of Bell's inequality under strict Einstein locality conditions, Phys. Rev. Lett. **81**, 5039 (1998).

[3] B. Hensen, H. Bernien, A. E. Dréau, A. Reiserer, N. Kalb, M. S. Blok, J. Ruitenberg, R. F. L. Vermeulen, R. N. Schouten, C. Abellán, W. Amaya, V. Pruneri, M. W. Mitchell, M. Markham, D. J. Twitchen, D. Elkouss, S. Wehner, T. H. Taminiau, and R. Hanson, Loophole-free Bell inequality violation using electron spins separated by 1.3 kilometres, Nature (London) **526**, 682 (2015).

[4] J. Yin, Y. Cao, Y. Li, S. Liao, L. Zhang, J. Ren, W. Cai, W. Liu, B. Li, H. Dai *et al.*, Satellite-based entanglement distribution over 1200 kilometers, Science **356**, 1140 (2017).

[5] D. Bouwmeester, J. Pan, K. Mattle, M. Eibl, H. Weinfurter, and A. Zeilinger, Experimental quantum teleportation, Nature (London) **390**, 575 (1997).

[6] A. Furusawa, J. L. Sørensen, S. L. Braunstein, C. A. Fuchs, H. J. Kimble, and E. S. Polzik, Unconditional quantum teleportation, Science **282**, 706 (1998).

[7] N. Lee, H. Benichi, Y. Takeno, S. Takeda, J. Webb, E. Huntington, and A. Furusawa, Teleportation of nonclassical wave packets of light, Science **332**, 330 (2011).

[8] S. L. Braunstein and H. J. Kimble, Dense coding for continuous variables, Phys. Rev. A **61**, 042302 (2000).

[9] X. Li, Q. Pan, J. Jing, J. Zhang, C. Xie, and K. Peng, Quantum dense coding exploiting a bright Einstein-Podolsky-Rosen beam, Phys. Rev. Lett. **88**, 047904 (2002).

[10] K. S. Chou, J. Z. Blumoff, C. S. Wang, P. C. Reinhold, C. J. Axline, Yvonne Y. Gao, L. Frunzio, M. H. Devoret, L. Jiang, and R. J. Schoelkopf, Deterministic teleportation of a quantum gate between two logical qubit, Nature (London) **561**, 368 (2018).

[11] X. Guo, C. R. Breum, J. Borregaard, S. Izumi, M. V. Larsen, T. Gehring, M. Christandl, J. S. Neergaard-Nielsen, and U. L. Andersen, Distributed quantum sensing in a continuous variable entangled network, Nat. Phys. **16**, 281 (2020).

[12] G. Masada and A. Furusawa, On-chip continuous-variable quantum entanglement, Nanophotonics **5**, 469 (2016).

[13] H. Chrzanowski, N. Walk, S. Assad, J. Janousek, S. Hosseini, T. Ralph, T. Symu, and P. Lan, Measurement-based noiseless linear amplification for quantum communication, Nat. Photonics **8**, 333 (2014).

[14] A. Ulanov, I. Fedorov, A. Pushkina, Y. Kurochkin, T. Ralph, and A. Lvovsky, Undoing the effect of loss on quantum entanglement, Nat. Photonics **9**, 764 (2015).

[15] T. Opatrný, G. Kurizki, and D. G. Welsch, Improvement on teleportation of continuous variables by photon subtraction via conditional measurement, Phys. Rev. A **61**, 032302 (2000).

[16] P. T. Cochrane, T. C. Ralph, and G. J. Milburn, Teleportation improvement by conditional measurements on the two-mode squeezed vacuum, Phys. Rev. A **65**, 062306 (2002).

[17] K. Akira, T. Masahiro, S. Masahide, and C. Anthony, Entanglement evaluation of non-Gaussian states generated by photon subtraction from squeezed states, Phys. Rev. A **73**, 042310 (2006).

[18] H. Takahashi, J. S. Neergaard-Nielsen, M. Takeuchi, M. Takeoka, K. Hayasaka, A. Furusawa, and M. Sasaki, Entanglement distillation from Gaussian input states, Nat. Photon. **4**, 178 (2010).

[19] L. Hu, Z. Liao, and M. S. Zubairy, Continuous-variable entanglement via multiphoton catalysis, Phys. Rev. A **95**, 012310 (2017).

[20] X. Xu, L. Hu, and Z. Liao, Improvement of entanglement via quantum scissors, J. Opt. Soc. Am. B **35**, 174 (2018).

[21] A. Ourjoumtsev, A. Dantan, R. Tualle-Brouri, and P. Grangier, Phys. Rev. Lett. **98**, 030502 (2007).

[22] G. Vidal and R. F. Werner, Computable measure of entanglement, Phys. Rev. A **65**, 032314 (2002).

[23] M. B. Plenio and S. S. Virmani, An introduction to entanglement theory, *Quantum Information and Coherence* (Springer, Cham, 2014), pp. 173–209.

[24] M. Dakna, T. Anhut, T. Opatrny, L. Knöll, and D. G. Welsch, Generation Schrödinger-cat-like states by means of conditional measurements on a beam splitter, Phys. Rev. A **55**, 3184 (1997).

[25] A. Ourjoumtsev, R. Tualle-Brouri, J. Laurat, and P. Grangier, Generating optical Schrödinger kittens for quantum information processing, Science **312**, 83 (2006).

[26] J. S. Neergaard-Nielsen, B. Melholt Nielsen, C. Hettich, K. Mølmer, and E. S. Polzik, Generation of a superposition of odd photon number states for quantum information networks, Phys. Rev. Lett. **97**, 083604 (2006).

[27] H. Song, G. Zhang, X. Wang, H. Yonezawa, and K. Fan, Amplification of optical Schrödinger cat states with an implementation protocol based on a frequency comb, Phys. Rev. A **105**, 043713 (2022).

[28] G. Zhang and M. R. James, On the response of quantum linear systems to single photon input fields, IEEE Trans. Autom. Control **58**, 1221 (2013).

[29] G. Zhang, Analysis of quantum linear systems' response to multi-photon states, Automatica **50**, 442 (2014).

[30] G. Zhang, Dynamical analysis of quantum linear systems driven by multi-channel multi-photon states, Automatica **83**, 186 (2017).

[31] G. Zhang and Z. Dong, Linear quantum systems: A tutorial, Annu. Rev. Control **54**, 274 (2022).

[32] C. H. Bennett, H. J. Bernstein, S. Popescu, and B. Schumacher, Concentrating partial entanglement by local operations, Phys. Rev. A **53**, 2046 (1996).

[33] H. Song, G. Zhang, and H. Yonezawa, Entanglement generation with Schrüdinger kitten states, in *2022 Asia Communications and Photonics Conference (ACP), Shenzhen, China* (IEEE, Piscataway, NJ, 2022), pp. 2135–2136.

[34] H. Shapourian, R. S. K. Mong, and S. Ryu, Anyonic partial transpose I: Quantum information aspects, arXiv:2012.02222.

[35] A. M. Branczyk and T. C. Ralph, Teleportation using squeezed single photons, Phys. Rev. A **78**, 052304 (2008).

[36] H. Song, K. B. Kuntz, and E. H. Huntington, Limitations on the quantum non-Gaussian characteristic of Schrödinger kitten state generation, New J. Phys. **15**, 023042 (2013).

[37] D. Fukuda, G. Fujii, T. Numata, K. Amemiya, A. Yoshizawa, H. Tsuchida, H. Fujino, H. Ishiii, T. Itatani, S. Inour, and T. Zama, Titanium-based transition-edge photon number resolving detector with 98% detection efficiency with index-matched small-gap fiber coupling, Opt. Express **19**, 870 (2011).

[38] Y. Takeno, M. Yukawa, H. Yonezawa, and A. Furusawa, Observation of −9 dB quadrature squeezing with improvement of phase stability in homodyne measurement, Opt. Express **15**, 4321 (2007).

[39] A. Schönbeck, F. Thies, and R. Schnabel, 13 dB squeezed vacuum states at 1550 nm from 12 mW external pump power at 775 nm, Opt. Lett. **43**, 110 (2017).